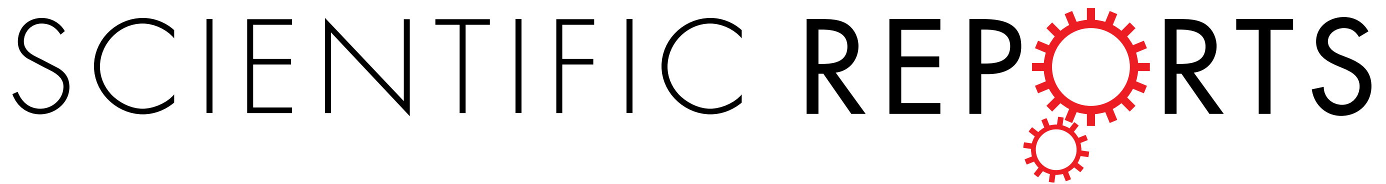

OPEN

Received: 08 June 2016
Accepted: 17 August 2016
Published: 15 September 2016

Decoupling the refractive index from the electrical properties of transparent conducting oxides via periodic superlattices

David Caffrey[1,2,3], Emma Norton[1,3], Cormac Ó Coileáin[1,3,4,5], Christopher M. Smith[1], Brendan Bulfin[6], Leo Farrell[1,3], Igor V. Shvets[1,2,3] & Karsten Fleischer[1,2,3]

We demonstrate an alternative approach to tuning the refractive index of materials. Current methodologies for tuning the refractive index of a material often result in undesirable changes to the structural or optoelectronic properties. By artificially layering a transparent conducting oxide with a lower refractive index material the overall film retains a desirable conductivity and mobility while acting optically as an effective medium with a modified refractive index. Calculations indicate that, with our refractive index change of 0.2, a significant reduction of reflective losses could be obtained by the utilisation of these structures in optoelectronic devices. Beyond this, periodic superlattice structures present a solution to decouple physical properties where the underlying electronic interaction is governed by different length scales.

A medium's refractive index (n) describes how the oscillating electric field of a light wave causes the disturbance of electrons which subsequently emit light. This emitted light will be out of phase with the original incident wave and cause interference. This results in an apparent reduction of the rate of propagation of light through the medium and hence a refractive index >1. The Fresnel equation describe that light incident upon an interface experiences reflection proportional to the refractive index mismatch of the two mediums. Thus matching of the refractive index of successive media is important if transmission is to be maximised.

Changing the refractive index of a medium as a whole is possible via temperature, mechanically induced strain, piezoelectricity and the introduction of porosity into the material[1]. Despite this, for typical optical applications, it is easier to replace a material with one of higher or lower refractive index rather than modifying the refractive index of a given material. The situation is more complex if the choice of material is governed by more than just the refractive index.

This is most apparent in the current generation of Transparent Conducting Oxides (TCOs), where the key requirements are high optical transparency and electrical conductivity. Only a small number of employable materials are currently known. Thus, the selection of a TCO with an optimal refractive index for a given device is often not feasible. This leads to significant unwanted reflection losses at the TCO and its interfaces in transparent devices, such as solar cells or displays. Developing a strategy to tune a TCO's refractive index is important to improve many optoelectronic devices.

Modifying the refractive index while retaining the conductivity and mobility is difficult as both properties are intertwined with the electron density of the material. One of the leading methodologies for the tuning of n is cation substitution, wherein atoms of a material are replaced by those of a lower electron density material. This results in an overall reduction of the electron density of the medium and hence, the refractive index.

An example of such is ZnO:Al, one of the leading low cost alternatives to Indium Tin Oxide (ITO)[2–6]. It has been demonstrated that by substituting controlled amounts of Mg for Zn in ZnO:Al to form $Zn_{1-x}Mg_xO$:Al

[1]School of Physics, Trinity College Dublin, Dublin 2, Ireland. [2]Advanced Materials Bio-Engineering Research Centre (AMBER), Trinity College Dublin, Dublin 2, Ireland. [3]Centre for Research on Adaptive Nanostructures and Nanodevices (CRANN), Trinity College Dublin, Dublin 2, Ireland. [4]KSU-Aramco Center, King Saud University, Riyadh 11451, Saudi Arabia. [5]School of Physics, Beijing Institute of Technology, Beijing 100081, P. R. China. [6]Institute of Solar Research, German Aerospace Center (DLR), 51147 Köln, Germany. Correspondence and requests for materials should be addressed to D.C. (email: dcaffrey@tcd.ie)

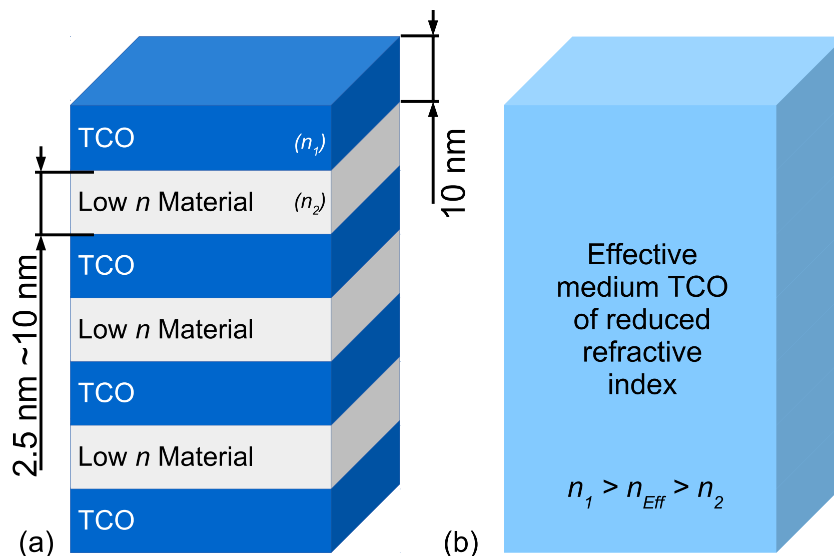

Figure 1. Conceptual Schematic of Superlattice. (**a**) The structure of the superlattices. (TCO layers (n_1) of 10 nm interspersed with low n (n_2) layers of 2.5 nm to 10 nm thickness). (**b**) The optical response of the superlattice, namely an effective medium of refractive index index $n_1 > n > n_2$.

the refractive index and optical bandgap of the material can be tuned[7–15]. Manipulation of the refractive index via cation substitution comes with significant repercussions. Increases in neutral impurity scattering originating from the implanted dopants leads to a reduction in mobility and conductivity of the films[7,9,11] and the high cation inclusion levels required can lead to dephasing[7,9]. These detrimental effects mean that an alternative method of tuning the refractive index without loss of the electrical properties is highly desirable.

In this work, we demonstrate the use of a superlattice composed of alternating thin pseudo 2D layers of a TCO and a lower electron density material. The confinement of the low refractive index material to layers substantially thinner than the wavelength of visible light results in a structure which behaves electronically as a set of successive conductive layers and optically as a medium equivalent to a mixture of the constituent materials. Thus the refractive index is effectively decoupled from the electrical properties, allowing for substantial changes while maintaining the high qualities of the TCO. This concept is illustrated in Fig. 1.

Oxide superlattices themselves have been previously well studied for other properties. Naturally occurring structures in layered oxides can induce variation in properties such as the photoluminescence[16], crystalline quality[17] and thermoelectric properties[18,19]. Artificial superlattices can optimise, enhance or tune the optical bandgap[20], oxidisation states[21], resistive switching[22], thermoelectric properties[23–26], TFTs[27] and ferroelectric properties[28–31].

Prominent n-type TCOs, amorphous $InGaZnO_4$ (a-IGZO) and ZnO:Al, were selected as the TCO layers alongside SiO_x as the low refractive index layer. ZnO:Al was selected as a TCO layer in order to facilitate direct comparison with previously mentioned results obtained via cation substitution of Mg. a-IGZO was selected as a result of its nature as a high mobility n-type TCO, with a number of properties contrasting with those of ZnO:Al. These include the nature of the crystallographic order of the materials (amorphous vs. crystalline) and the variation in their carrier generation mechanisms (intrinsic vs. extrinsic)[3,32,33].

SiO_x was selected for its cost effectiveness and low refractive index ($n \approx 1.45$) to facilitate tuning over a wide range of values. Increasing n by inclusion of dielectric layers with higher refractive index than the host TCO is equally feasible to the reduction of n described in this work.

Beyond this, modifications such as combining high carrier concentration doping layers with high mobility transport layers are theoretically possible by employing this concept. In addition, the above could be combined with the inducement of optical band gap shifts (as shown for a-IGZO by Abe *et al.*[20]) by selection of appropriate periodicity and functionalisation layer for confinement effects.

Results

Properties of a TCO/Dielectric superlattice. The deposited superlattices consisted of 10 nm TCO layers (either a-IGZO or ZnO:Al) interspersed with SiO_x layers of thickness 2–10 nm. The periodic nature of the layered structure of the superlattices was confirmed via cross-sectional Scanning Electron Microscopy (SEM). Representative images of the superlattices deposited in this work are provided in Fig. 2. X-Ray Reflectivity (XRR) measurements were fitted to obtain the average individual layer thickness of the deposited films. Further details of the characterisation of the deposited superlattices are given in the supplementary information including fits of the XRR data (Supplement S1 and S7). X-Ray Diffraction (XRD) of the superlattices demonstrated the a-IGZO to be amorphous and ZnO:Al to be crystalline for all samples (see Supplement S2).

The mobility and conductivity of the a-IGZO and ZnO:Al superlattices are plotted as a function of refractive index in Fig. 3. Values obtained previously for cation substitution in $Zn_{1-x}Mg_xO$:Al[7] are plotted for comparison.

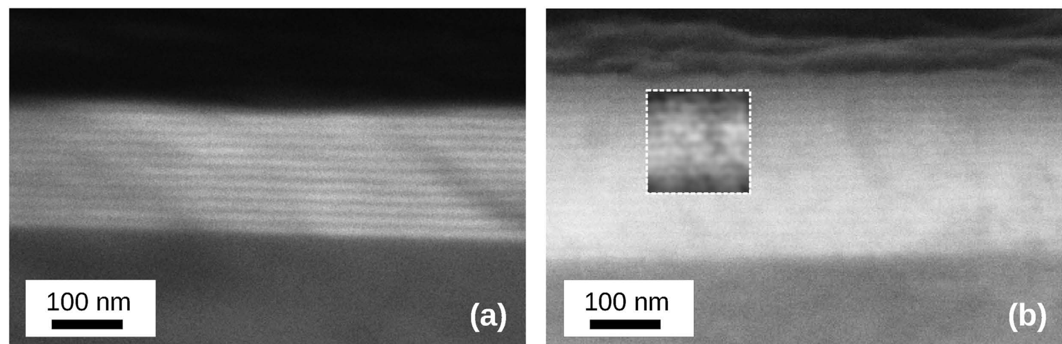

Figure 2. Cross-sectional SEM of of TCO/SiO_x superlattices. Cross sectional image of (**a**) 10/7.5 nm a-IGZO/SiO_x and (**b**) 10/5 nm ZnO:Al/SiO_x superlattices on glass substrate (**a**) was obtained using a backscatter electron detector and (**b**) with a secondary electron detector. Inset of (**b**) has been post processed to locally enhance contrast within the layered structure.

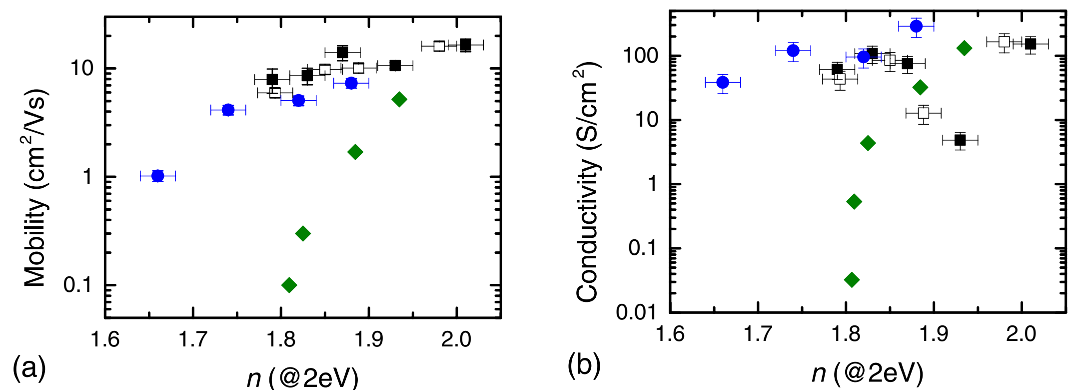

Figure 3. Mobility vs. *n* of the deposited Superlattices. Modulation in the (**a**) mobility and (**b**) conductivity of the superlattices plotted against their refractive index at $h\nu = 2$ eV ($\lambda = 620$ nm). Results for cation substituted $Zn_{1-x}Mg_xO$:Al are included for comparison. (■) a-IGZO/SiO_x superlattices on glass substrate, (□) a-IGZO/SiO_x superlattices on Al_2O_3, (●) ZnO:Al/SiO_x superlattices, (♦) $Zn_{1-x}Mg_xO$:Al grown by spray pyrolysis from Fleischer *et al.*[7].

The refractive index was taken in the middle of the visible range (2 eV) for all samples. The refractive index of the films was found to decrease systematically with increasing SiO_x layer thickness, for both a-IGZO/SiO_x (1.97 to 1.75) and ZnO:Al/SiO_x (1.88 to 1.66) superlattices, while maintaining high mobility and conductivity. The robustness of the method was demonstrated by the consistency in the mobility and conductivity between superlattices deposited on standard microscope slides and those deposited on polished sapphire. This illustrates that no special choice of smooth substrate is required for the efficacy of the superlattices.

It should be noted that we found that, for our deposition conditions, the atomic composition of a thin a-IGZO layer (10 nm) slightly differs from a thicker one (100 nm). However, this small change did not alter the mobility of these films. Within the superlattice the composition of the individual a-IGZO layers does not vary and is similar to a single 10 nm film. Full details of the compositional analysis are given in supplementary information (Supplement S3). As can be seen from Fig. 3(a), both a-IGZO/SiO_x and ZnO:Al/SiO_x superlattice structures are found to maintain significantly higher mobility with tuned refractive indices than for equivalent films obtained previously with cation substitution of ZnO:Al with Mg[7]. In Fig. 3(b), a similar improvement is seen in the conservation of the conductivity of the superstructures, with a reduction of less than an order of magnitude observed in both cases, while cation substitution exhibited significantly greater reductions with a narrower tunable refractive index range.

On a macroscopic scale it is intuitive that structures consisting of layered conductive and non-conductive materials will lead to a significant increase in the out of plane serial resistance of the structure, resulting in a conduction anisotropy $\sigma_{x,y} > \sigma_z$. However, on the nano-scale such assumptions can be deceptive and the situation becomes more complicated as the thickness of the individual layers within the superstructure are reduced towards the order of the electron mean free path. In such cases, this will not solely depend on the resistivity of the material but also on the nature of its bandstructure, in particular the conduction band offset relative to the TCO layers, allowing for further optimisation from an electrical point of view. As a result, in low dimensional superlattices consisting of conductive and non-conductive layers it is important to establish that conduction occurs throughout the superstructure. Should the current be unable to penetrate into the lower layers of the superlattices a sharp

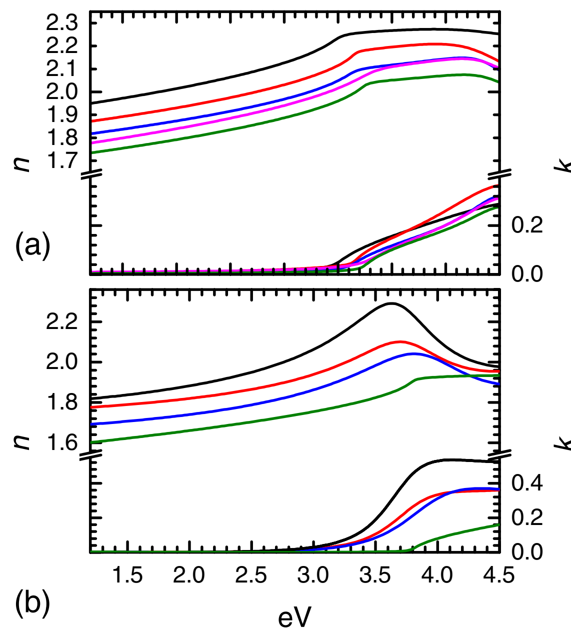

Figure 4. Refractive index of the superlattices. Dielectric functions of the (**a**) a-IGZO/SiO_x and (**b**) ZnO:Al/SiO_x superlattices. (–) bulk film, (—) 10/**2.5 nm**, (—) 10/**5 nm**, (—) 10/**7.5 nm**, (—) 10/**10 nm**.

decrease in the conductivity with increasing SiO_x layer thickness would be expected as the conduction is limited to the topmost TCO layers. This is not seen in our samples. By comparing two 10/10 a-IGZO/SiO_x superlattices of different overall thickness (90 nm and 190 nm) and a reference 10 nm a-IGZO film this was further confirmed. A full discussion of these samples and their characterisation can be found in the supplementary information (Supplement S3).

Finite Element Method (FEM) simulations were performed to assess under which condition the current density would be homogeneously distributed over all individual TCO layers. It was found that for the thickest SiO_x layers (10 nm) this is achieved for SiO_x resistivities of less than 10^6 Ωcm. For highly resistive SiO_x the current would be partially limited to the first few TCO layers. This simulation underestimates the current injection in two notable ways; firstly, it does not take into account non-classical effects, which are expected once the SiO_x layer thickness approaches the electron mean free path. In this case tunneling should increase the current injection. Secondly, there is evidence that the deposited SiO_x is understoichiometric and defective, making it less insulating than bulk SiO_2[34]. A full discussion of the FEM simulations can be found in the supplementary information (Supplement S5). From these simulations and the above experimental observations we can conclude that the current is distributed throughout the superstructure. The discussions above highlight that careful choice of material is key for attainment of optimal electrical properties of the superlattices.

The effective refractive indices of the superlattices are given in Fig. 4. In both cases a clear reduction of the real part of the refractive index of the superlattice is observed with increasing SiO_x layer thickness. The range over which the refractive index could be tuned was expanded relative to cation substitution. Via the use of superlattices a $\Delta n \approx 0.2$ is observed in our films with a reduction of less than an order of magnitude in the conductivity, whereas in cation substitution the change was limited to $\Delta n \approx 0.13$ accompanied by a several orders of magnitude degradation of the conductivity. The transmission spectrum of the superlattices is plotted in Fig. 5. Transmission in the visible spectrum remains in the 80–90% range for all samples, with variation originating from changes in the Fabry-Pérot oscillations due to slight thickness deviations and, more significantly, the refractive index change.

Concerning possible electronic confinement effects within the IGZO layers, we observed in both sets of superlattices some shifts in the position of the fitted bulk critical point which can be related to the band gap energy. It has been previously shown that the a-IGZO/SiO_2 band offset can lead to strong confinement[35], although it would be expected that thinner a-IGZO layers than used in this work would be required to induce quantisation[20]. Due to alterations in the shape of the high energy extinction coefficient (k) complicating analysis, it is difficult to explicitly interpret these critical point shifts as an indication of the alteration of the optical band gap. This is further discussed in the supplementary information (Supplement S6).

In this work SiO_x was employed as the low index layer due to its comparatively low index ≈1.45 and industrial relevance. However, the concept of engineering the refractive index by using superlattice structures is largely material independent. Many TCO-functional layer combinations are yet to be explored. For instance the range of tunability of the refractive index can be improved upon by replacing SiO_x with a material of lower electron density. An example of such would be MgF_2 ($n \approx 1.37$) a transparent material currently employed as an anti-reflective layer on crown glass[36,37]. The use of such a low index layer would facilitate tuning of the refractive index over a wider range than that described above.

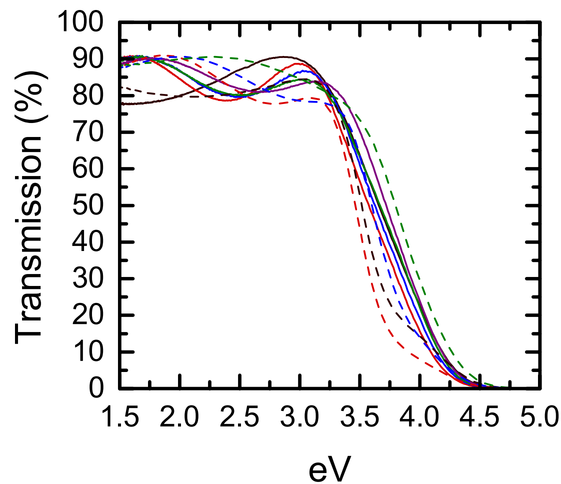

Figure 5. Transmission of the a-IGZO and ZnO:Al based superlattices. (—) 100 nm a-IGZO, (—) 10/**2.5 nm** a-IGZO/SiO_x superlattice, (—) 10/**5 nm** a-IGZO/SiO_x superlattice, (—) 10/**7.5 nm** a-IGZO/SiO_x superlattice, (—) 10/**10 nm**. a-IGZO/SiO_x superlattice, (---) 80 nm ZnO:Al, (- - -) 10/**2.5 nm** ZnO:Al/SiO_x superlattice, (- - -) 10/**5 nm** ZnO:Al/SiO_x superlattice, (- - -) 10/**10 nm** ZnO:Al/SiO_x superlattice.

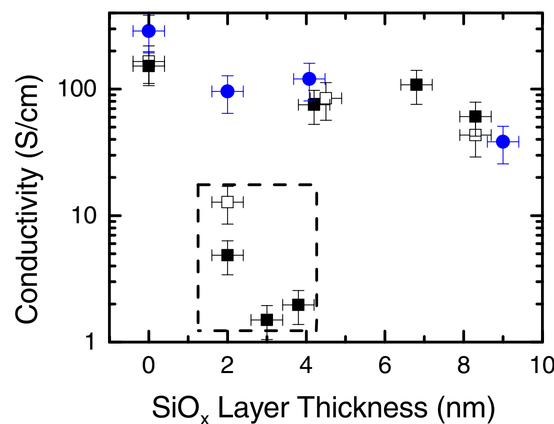

Figure 6. Conductivity of the superlattices as a function of the SiO_x layer thickness. Conductivity vs. SiO_x layer thickness of the a-IGZO/SiO_x superlattices and ZnO:Al/SiO_x superlattices. (■) a-IGZO/SiO_x superlattices on glass substrate, (□) a-IGZO/SiO_x superlattices on Al_2O_3, (●) ZnO:Al/SiO_x superlattices. The low thickness SiO_x layers exhibiting lower conductivities are highlighted by the dashed box.

Estimated impact of superlattice structures in devices. With the demonstrated tunability we can assess improvements in the light harvesting of a thin film solar cell by the same method as outlined previously by Fleischer *et al.*[38]. By utilising the dielectric function calculated in this work for the a-IGZO/SiO_x superlattices and assuming a similar structure could be grown for a high refractive index material, we can calculate the estimated reflective improvement using the Fresnel equations in a transfer matrix calculation. For the glass/FTO/a-Si/Al thin film solar cell considered there, the use of the tuned TCO superlattice can modestly increase the conversion efficiency by ~2%. If our tuning concept is further developed to high index materials e.g. by using TiO_2/IGZO superlattices and assuming that a similar structure can be grown, the refractive index could be expected to increase up to ~2.3. This would reduce internal reflections in the discussed solar cell structure at the TCO/absorber interface increasing conversion efficiency by up to 9%. By combining both internal high index and low index anti-reflective TCO superlattices improvements of up to 11% could be obtained.

In much simpler structures such as conductive transparent coatings (e.g. in displays) the overall reflection from the TCO layer can also be reduced employing the superlattice concept. For example the reflectance of a typical 500 nm ZnO:Al film on glass can be reduced from average values in the visible range of 10% to 7% and 6% using a 10/5 or 10/10 ZnO:Al/SiO_x superlattice respectively.

Anomalous behavior of low SiO_x layer thickness a-IGZO/SiO_x superlattices. It can be observed in Figs 3 and 6 that some superlattices experience an anomalous decrease in conductivity. This occurs in a-IGZO superlattices with an SiO_x layer thickness below 4 nm. XRR and XRD of the thin films confirm that increased

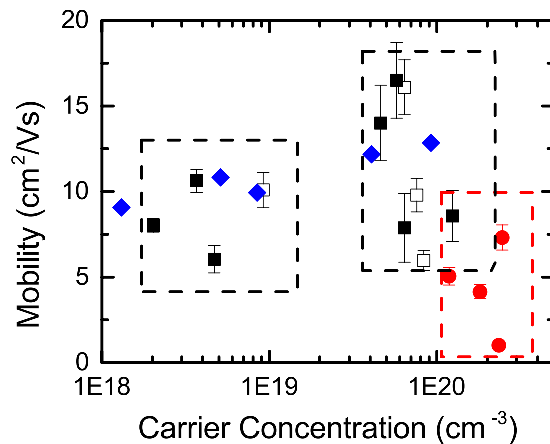

Figure 7. Mobility vs. carrier concentration. Variation in the carrier concentration of the superlattices with SiO_x layer thickness. (■) a-IGZO/SiO_x superlattices on glass substrate, (□) a-IGZO/SiO_x superlattices on Al_2O_3, (●) ZnO:Al/SiO_x superlattices, (⋆) Values for bulk a-IGZO from Akihiro Takagi *et al.*[39]. The behaviour of the films can be categorised into three regions. Region A consists of the a-IGZO superlattices with SiO_x layers of 2–4 nm thickness. Region B consists of the a-IGZO superlattices with SiO_x layers of 4–10 nm thickness. Region C consists of the a-ZnO:Al superlattices. Variation of the mobility within these regions is a result of the modulation of the SiO_x thickness over the specified range.

roughness at low thicknesses is not a factor. This is intuitive as such would be expected to enhance conductivity due to contact between successive a-IGZO layers. The origin is thus likely to be some electronic property of the a-IGZO or SiO_x at developed at low thicknesses. Direct measurement of the origin of this behavior would require *in-situ* analysis of the properties of the SiO_x layers during growth, as exposure to atmospheric conductions introduces contaminants that either compensate for or mask the effect. Such methods were not available during the growth of these superlattices and as such, we must rely on indirect evidence to gain insight into the nature of this effect.

Significant variation is observed in the carrier concentration of the films. Figure 7 depicts the mobility of the superlattices as a function of their carrier concentration alongside results obtained for standard a-IGZO films deposited at varied oxygen partial pressures by Takagi *et al.*[39]. Two distinct regions can be identified. Region A, consisting of superlattices of SiO_x layer thickness >4 nm, and region B, consisting of those of <4 nm alongside the bulk a-IGZO films. It can be noted that the ZnO:Al/SiO_x superlattices, as shown in Figs 6 and 7 (region C), do not show these variations. In order to understand the possible origins of this we can address the fundamental carrier generation mechanisms of ZnO:Al and a-IGZO. The majority carriers in ZnO:Al are known to originate from the extrinsic substitution of Al on the Zn site[40,41]. In contrast, the donor defect in a-IGZO is widely considered to be strongly tied to intrinsic oxygen vacancy defects, resulting in the carrier concentration being oxygen sensitive[39,42–44]. As a result, while both materials are sensitive to oxygen within their structure, due to oxygen interstitials acting as electron pinning defects, it is expected that the a-IGZO would show a significantly higher sensitivity. Thus by considering the similarity of the behavior of the a-IGZO to that deposited at varying partial pressures of oxygen and the difference in the behavior of the ZnO:Al and a-IGZO superlattices, we tentatively ascribe this behavior to variation in the oxygen environment during growth or in the deposited superlattices.

We believe that such variation in oxygen could be explained by the properties of low thickness SiO_x. It has been demonstrated that the formation energy of defect can be enhanced for thin SiO_x layers as deposited here[34,45,46]. We theorise that the root cause of the observed changes in the a-IGZO layers is most likely an altered defect density for ultrathin SiO_x layers leading to a locally changed oxygen structure. This could take the form of variation in the local oxygen partial pressure near the surface of the growing film or enhanced oxygen/cation interlayer diffusion induced by the under-stoichiometric SiO_x surface. This diffusion could take the form of either Si diffusion, which has been shown to act as a carrier suppressor in amorphous InZnO and IGZO[47,48], or oxygen vacancies, which are heavily tied to the donor defect structure of a-IGZO[39,42–44].

We thus believe that the indirect evidence as outlined above supports the conclusion that the change in the electrical properties of the films is related to the formation of defective SiO_x at low thicknesses. In order to verify this a precise methodology for *in-situ* measurement of the properties of the interface during growth, such as combination of *in-situ* XPS and magnetron sputtering, would be required.

Conclusion

a-IGZO/SiO_x and ZnO:Al/SiO_x superlattices were deposited to decouple the value of the refractive index of the films while maintaining the optoelectronic properties.

By varying the thickness of the periodic SiO_x layers the refractive index of a-IGZO and ZnO:Al were tuned by $\Delta n \approx 0.2$. Over this refractive index change, the mobility for the a-IGZO and ZnO:Al superlattices varied from 16.5 cm^2/Vs to 6 cm^2/Vs and 7.3 cm^2/Vs to 1 cm^2/Vs respectively. Conductivity was found to be maintained within an order of magnitude of the original values. Selection of an appropriate tuning material is key to attaining strong conservation of the electrical properties and it is believed that by careful choice of refractive index tuning

layer this methodology could be expanded to other materials to produce further optimised results in terms of conductivity and refractive index.

In terms of possible applications, we calculated that a reduction of 10% to 6% in reflected losses are expected if this technique is applied to transparent conducting optical coatings.

We believe that the discussed results demonstrate the great potential for this superlattice based technique, not just to dissociate the optical and electrical properties, but also for the decoupling of other physical quantities where the atomic interactions are governed by different length scales.

Methods

Sample preparation. Samples were deposited via Radio Frequency (RF) magnetron sputtering via co-sputtering from separate 2 inch diameter InGaZnO (a-IGZO), ZnO:Al (2 at% Al) and SiO_2 targets. Targets were sputtered sequentially in order to produce a layered structure. 100 W of power was applied to the a-IGZO and SiO_2 targets during deposition while ZnO:Al was sputtered using 50 W. Power to the TCO target was ramped down between successive layers in order to maintain a consistent composition throughout the superlattice. Nominal elemental composition of the a-IGZO target was 1:1:1:4 (In:Ga:Zn:O) as confirmed by Energy Dispersive X-ray (EDX) spectroscopy. The sputtering chamber was evacuated to below 10^{-2} Pa prior to deposition, then backfilled with 0.45 Pa of Ar during sputtering. Films were deposited onto Menzel-Glaser glass microscope slides and polished c-plane aligned sapphire supplied by CrysTec. Substrates were ultrasonically cleaned in acetone and isopropanol prior to deposition. Samples were deposited at a substrate temperature of 450 °C. This temperature was selected to maximise conductivity, while maintaining the amorphous nature of the a-IGZO. Growth rates of the films were determined via XRR and ellipsometry measurements of representative samples. Superstructures of varying SiO_x layer thickness were deposited by controlling the SiO_x layer growth time. Superlattices were grown to a total thickness of 150–200 nm in order to facilitate optical comparison between samples. Films were capped with 10 nm of the TCO layer in order to facilitate electrical contacting. The structure obtained for each superlattice can be found in the supplementary information (Supplement S7).

Post Treatment. Films were annealed in a nitrogen atmosphere at 320 °C for highest conductivity, with properties being measured *in situ* via 4 point probe in linear configuration. The typical improvement in conductivity of the films was approximately an order of magnitude in both cases.

X-Ray-Diffraction. XRD patterns have been measured with a *Bruker D8 Advance* using a Mo-Kα source. Crystal phase and orientation of the ZnO:Al/SiO_x superlattices were obtained using *Bruker*'s EVA program. Crystallite size was obtained using the Scherrer equation.

X-Ray-Reflectivity. X-Ray Reflection (XRR) measurements obtained with a *Bruker D8 Discover* equipped with a monochromised Cu-Kα source were fitted using the *Bruker* Leptos program in order to obtain the average thickness of the TCO and dielectric layers and density of the films.

Scanning Electron Microscopy. Cross-sectional Scanning Electron Microscopy (SEM) was performed using a *Carl Zeiss Ultra*. Samples were cleaved prior to scanning in order to present a clean edge for imaging. All images were obtained at 5 keV to enhance the signal from the surface. The a-IGZO/SiO_x superlattices were imaged using the backscatter electron detector which produced a high contrast due to the significant variation in Z between a-IGZO and SiO_x. The ZnO:Al/SiO_x superlattices were imaged using the secondary electron detector. Images of the ZnO:Al/SiO_x superlattices were complicated by the comparitively low Z contrast between layers. To compensate for this, post-processing was performed on a portion of the image to smooth and maximise contrast, as shown in the inset of Fig. 2(b). Unfortunately there is additional contrast within the ZnO:Al layers due to their polycrystalline nature. This results in a rougher cleavage plane than that obtained for the a-IGZO film.

Optical Analysis. UV Visible spectrophotometry (*Lambda 650S Perkin Elmer*) was used to measure the transmission and reflectance of the films. Films were scanned from 1.5–5 eV. The absorption coefficient (α) was calculated from the transmission and reflectance data using equation 1.

$$\alpha = \frac{-\ln(T + R)}{t} \tag{1}$$

where T and R are the transmission and reflectance of the films respectively at a given energy and t is the thickness of the films. Tauc plots of $\alpha^{-n}h\nu$ vs. $h\nu$, where n = 1/2 for direct band semiconductors, were performed on a-IGZO with sapphire substrates in order to determine the optical band gap. Tauc plots of the samples deposited on glass were complicated by the coincidence of the onset of absorption of the TCO and glass substrate. The refractive index was obtained via variable angle spectroscopic ellipsometry (*Sopra GESP 5*). Measurements were obtained at angles close to the pseudo Brewster Angle of 62, 65 and 68 for a-IGZO and 59, 62, 65 for ZnO:Al. The superstructures were modeled as an effective medium with a critical point and UV oscillator to accurately describe the high transmission and onset of absorption. The refractive indices of the a-IGZO/SiO_x superlattices were modeled by use of a 3D critical point alongside a UV oscillator fixed at 5 eV, while for the ZnO:Al/SiO_x superlattices a 1D critical point alongside a UV oscillator was employed. Values of the overall thickness of the superlattices obtained from the ellipsometry fits were found to be consistent with those obtained via XRR further confirming the validity of the model. Decoherence in the reflected light resulting from increased roughness at the ZnO:Al/SiO_x interface leads to a significant reduction in the resolution of our measurement in the high energy range for the 10/10 ZnO:Al/SiO_x superlattice. Refractive index of the bulk a-IGZO and ZnO:Al were found to

be increased and reduced respectively relative to database values due to density variations present in the samples (See discussion of XRR in Supplement S1 for details).

Electrical characterisation. Mobility and conductivity of the samples were obtained via Hall measurements performed using silver adhesive contacts arranged in a Van der Pauw configuration in conjunction with a 10 T field in a Physical Property Measurement System (*Quantum Design*). Forward and reverse bias measurements were taken in all directions to minimise any geometry or sample inhomogeneity based errors. Electrical properties, such as conductivity, were calculated using the overall thickness of the superlattice, including the SiO_x layers. Carrier concentration was calculated using only the combined thickness of the TCO layers.

References

1. Shen, J. *et al.* Low dielectric constant silica films with ordered nanoporous structure. *Mater. Sci. Eng. C* **27,** 1145–1148 (2007).
2. Özgür, Ü. *et al.* A comprehensive review of ZnO materials and devices. *J. Appl. Phys.* **98,** 041301 (2005).
3. Ellmer, K. Resistivity of polycrystalline zinc oxide films: current status and physical limit. *J. Phys. D: Appl. Phys.* **34,** 3097 (2001).
4. Ellmer, K. Past achievements and future challenges in the development of optically transparent electrodes. *Nat. Photonics* **6,** 809–817 (2012).
5. Wang, Z. *et al.* Growth of ZnO:Al films by RF sputtering at room temperature for solar cell applications. *Solid-State Electron.* **53,** 1149–1153 (2009).
6. De Sio, A. *et al.* ITO-free inverted polymer solar cells with ZnO:Al cathodes and stable top anodes. *Sol. Energy Mater. Sol. Cells* **98,** 52–56 (2012).
7. Fleischer, K., Arca, E., Smith, C. & Shvets, I. Aluminium doped $Zn_{1-x}Mg_xO$ – A transparent conducting oxide with tunable optical and electrical properties. *Appl. Phys. Lett.* **101,** 121918 (2012).
8. Törndahl, T., Platzer-Björkman, C., Kessler, J. & Edoff, M. Atomic layer deposition of $Zn_{1-x}Mg_xO$ buffer layers for Cu (In, Ga) Se2 solar cells. *Prog. Photovoltaics Res. Appl.* **15,** 225–235 (2007).
9. Lu, J. G. *et al.* Carrier concentration induced band-gap shift in Al-doped $Zn_{1-x}Mg_xO$ thin films. *Appl. Phys. Lett.* **89,** 262107 (2006).
10. Ke, Y. *et al.* Enhanced Electron Mobility Due to Dopant-Defect Pairing in Conductive ZnMgO. *Adv. Funct. Mater.* **24,** 2875–2882 (2014).
11. Matsubara, K. *et al.* Band-gap modified Al-doped $Zn_{1-x}Mg_xO$ transparent conducting films deposited by pulsed laser deposition. *Appl. Phys. Lett.* **85,** 1374 (2004).
12. Minemoto, T., Negami, T., Nishiwaki, S., Takakura, H. & Hamakawa, Y. Preparation of $Zn_{1-x}Mg_xO$ films by radio frequency magnetron sputtering. *Thin Solid Films* **372,** 173–176 (2000).
13. Bikowski, A. & Ellmer, K. A comparative study of electronic and structural properties of polycrystalline and epitaxial magnetron-sputtered ZnO:Al and $Zn_{1-x}Mg_xO$:Al doped films. Origin of the grain barrier traps. *J. Appl. Phys.* **114,** 063709 (2013).
14. Ellmer, K. & Vollweiler, G. Electrical transport parameters of heavily-doped zinc oxide and zinc magnesium oxide single and multilayer films heteroepitaxially grown on oxide single crystals. *Thin Solid Films* **496,** 104–111 (2006).
15. Bikowski, A., Welzel, T. & Ellmer, K. The impact of negative oxygen ion bombardment on electronic and structural properties of magnetron sputtered ZnO:Al films. *Appl. Phys. Lett.* **102,** 242106 (2013).
16. Hiramatsu, H. *et al.* Layered mixed-anion compounds: epitaxial growth, active function exploration, and device application. *J. Eur. Ceram. Soc.* **29,** 245–253 (2009).
17. Cho, S. W., Kim, J. H., Shin, S., Cho, H. H. & Cho, H. K. All-solution-processed $InGaO_3 (ZnO)_m$ thin films with layered structure. *Journal of Nanomaterials* **2013,** 909786 (2013).
18. Kim, J. H. *et al.* Hybrid solution processed $InGaO_3 (ZnO)_m$ thin films with periodic layered structures and thermoelectric properties. *J. Mater. Chem.* **22,** 16312–16317 (2012).
19. Seo, D. K. *et al.* Drastic improvement of oxide thermoelectric performance using thermal and plasma treatments of the InGaZnO thin films grown by sputtering. *Acta Mater.* **59,** 6743–6750 (2011).
20. Abe, K., Nomura, K., Kamiya, T. & Hosono, H. Optical evidence for quantization in transparent amorphous oxide semiconductor superlattice. *Phys. Rev. B* **86,** 081202 (2012).
21. Matsumoto, K. *et al.* Selective reduction of layers at low temperature in artificial superlattice thin films. *Sci. Rep.* **1,** 27 (2011).
22. Choi, W. S., Lee, S. A., You, J. H., Lee, S. & Lee, H. N. Resonant tunnelling in a quantum oxide superlattice. *Nat. Commun.* **6,** 7424 (2015).
23. Venkatasubramanian, R., Siivola, E., Colpitts, T. & O'quinn, B. Thin-film thermoelectric devices with high room-temperature figures of merit. *Nature* **413,** 597–602 (2001).
24. Ohta, H. Two-dimensional thermoelectric Seebeck coefficient of $SrTiO_3$-based superlattices. *Phys. Stat. Sol. B* **245,** 2363–2368 (2008).
25. Zide, J. *et al.* Demonstration of electron filtering to increase the Seebeck coefficient in $In_{0.53}Ga_{0.47}As/In_{0.53}Ga_{0.28}Al_{0.19}As$ superlattices. *Phys. Rev. B* **74,** 205335 (2006).
26. Bulman, G. *et al.* Superlattice-based thin-film thermoelectric modules with high cooling fluxes. *Nat. Commun.* **7,** 10302 (2016).
27. Ahn, C. H., Senthil, K., Cho, H. K. & Lee, S. Y. Artificial semiconductor/insulator superlattice channel structure for high-performance oxide thin-film transistors. *Sci. Rep.* **3,** 2737 (2013).
28. Bein, B. *et al. In situ* X-ray diffraction and the evolution of polarization during the growth of ferroelectric superlattices. *Nat. Commun.* **6,** 10136 (2015).
29. Lee, H. N., Christen, H. M., Chisholm, M. F., Rouleau, C. M. & Lowndes, D. H. Strong polarization enhancement in asymmetric three-component ferroelectric superlattices. *Nature* **433,** 395–399 (2005).
30. Bousquet, E. *et al.* Improper ferroelectricity in perovskite oxide artificial superlattices. *Nature* **452,** 732–736 (2008).
31. Yadav, A. *et al.* Observation of polar vortices in oxide superlattices. *Nature* **530,** 198–201 (2016).
32. Nomura, K. *et al.* Room-temperature fabrication of transparent flexible thin-film transistors using amorphous oxide semiconductors. *Nature* **432,** 488–492 (2004).
33. Kamiya, T. & Hosono, H. Material characteristics and applications of transparent amorphous oxide semiconductors. *NPG Asia Materials* **2,** 15–22 (2010).
34. Eftekhari, G. Electrical conduction in rapidly annealed sputter-deposited SiO_2 films (in O_2 Ar atmosphere) on Si. *physica status solidi (a)* **151,** 129–133 (1995).
35. Douglas, E. *et al.* Measurement of $SiO_2/InZnGaO_4$ heterojunction band offsets by x-ray photoelectron spectroscopy. *Appl. Phys. Lett.* **98,** 2110 (2011).
36. Noack, J. *et al.* MgF_2 antireflective coatings by sol–gel processing: film preparation and thermal densification. *J. Mater. Chem.* **22,** 18535–18541 (2012).
37. Scheurell, K. *et al.* Optimisation of a sol–gel synthesis route for the preparation of MgF_2 particles for a large scale coating process. *Dalton Trans.* **44,** 19501–19508 (2015).

38. Fleischer, K., Arca, E. & Shvets, I. Improving solar cell efficiency with optically optimised TCO layers. *Sol. Energy Mater. Sol. Cells* **101,** 262–269 (2012).
39. Takagi, A. *et al.* Carrier transport and electronic structure in amorphous oxide semiconductor, a-$InGaZnO_4$. *Thin Solid Films* **486,** 38–41 (2005).
40. Gabás, M. *et al.* Unraveling the conduction mechanism of Al-doped ZnO films by valence band soft x-ray photoemission spectroscopy. *Appl. Phys. Lett.* **86,** 042104 (2005).
41. Ohashi, N. *et al.* Band-edge emission of undoped and doped ZnO single crystals at room temperature. *J. Appl. Phys.* **91,** 3658–3663 (2002).
42. Kamiya, T., Nomura, K., Hirano, M. & Hosono, H. Electronic structure of oxygen deficient amorphous oxide semiconductor a-$InGaZnO_{4-x}$: Optical analyses and first-principle calculations. *Phys. Stat. Sol. C* **5,** 3098–3100 (2008).
43. Nonaka, Y. *et al.* Investigation of defects in In–Ga–Zn oxide thin film using electron spin resonance signals. *J. Appl. Phys.* **115,** 163707 (2014).
44. Nakashima, M. *et al.* Origin of major donor states in In–Ga–Zn oxide. *J. Appl. Phys.* **116,** 213703 (2014).
45. Nadimi, E., Plänitz, P., Öttking, R., Schreiber, M. & Radehaus, C. Single and Multiple Oxygen Vacancies in Ultrathin Gate Dielectric and Their Influence on the Leakage Current: An Ab Initio Investigation. *Electron Device Letters, IEEE* **31,** 881–883 (2010).
46. Ghetti, A., Sangiorgi, E., Bude, J., Sorsch, T. & Weber, G. Low voltage tunneling in ultra-thin oxides: a monitor for interface states and degradation. In *Electron Devices Meeting, 1999. IEDM'99. Technical Digest. International*, 731–734 (IEEE, 1999).
47. Chong, E., Chun, Y. S. & Lee, S. Y. Amorphous silicon-indium-zinc oxide semiconductor thin film transistors processed below 150 C. *Appl. Phys. Lett.* **97,** 2102 (2010).
48. Lee, H.-R. & Park, J.-G. High-stability transparent amorphous oxide TFT with a silicon-doped back-channel layer. *Journal of the Korean Physical Society* **65,** 1174–1178 (2014).

Acknowledgements

This publication has emanated from research conducted with the financial support of Science Foundation Ireland (SFI) under Grant Number SFI/12/RC/2278 and 12/IA/1264. This work was also supported by the Higher Education Authority under the PRTLI scheme, cycle 5 and the Irish Research Council under Grant No. GOI/PG/2013/445. C.Ó.C. would like to thank Saudi Aramco (No. 6600028398) and KACST-National Project for Science and Technology (12-NAN2672-02) for the financial support.

Author Contributions

D.C. prepared all samples, wrote this article, performed the electrical measurements and optical fitting, XRR, XRD and SEM. E.N. performed all XPS measurements and analysis. C.Ó.C. performed all Hall measurements. C.M.S. performed optical measurements and aided in optical modeling. B.B. performed supporting finite element calculations to quantify the impact of the SiO_2 layers on the electrical measurements L.F. provided key conceptual insight. I.V.S. instigated and led the project. K.F. provided aid in optical modeling, theoretical and practical analysis of the results and was instrumental in outlining the experiments.

Additional Information

Supplementary information accompanies this paper at http://www.nature.com/srep

Competing financial interests: The authors declare no competing financial interests.

How to cite this article: Caffrey, D. *et al.* Decoupling the refractive index from the electrical properties of transparent conducting oxides via periodic superlattices. *Sci. Rep.* **6**, 33006; doi: 10.1038/srep33006 (2016).

This work is licensed under a Creative Commons Attribution 4.0 International License. The images or other third party material in this article are included in the article's Creative Commons license, unless indicated otherwise in the credit line; if the material is not included under the Creative Commons license, users will need to obtain permission from the license holder to reproduce the material. To view a copy of this license, visit http://creativecommons.org/licenses/by/4.0/

© The Author(s) 2016

Decoupling the refractive index from the electrical properties of transparent conducting oxides via periodic superlattices

David Caffrey, Emma Norton, Cormac Ó Coileáin, Christopher M. Smith, Brendan Bulfin, Leo Farrell, Igor V. Shvets, and Karsten Fleischer

Supplementary Information

S1. X-Ray Reflection measurements of the superlattices

X-Ray Reflectivity (XRR) analysis has previously been demonstrated to be an invaluable tool in the investigation of superlattice properties[1–5]. Here XRR was employed to confirm the thickness of the periodic layers, interface roughness and to obtain the density of the deposited material. The densities of the materials were obtained from measurements of representative samples of the films. The density of the deposited a-IGZO was found to be 6.8g/cm^3, higher than typically reported values[6]. This densification of the material can be attributed to the high level of indium enrichment of the films (see Supplement S3) in conjunction with the known effects of depositing at a low pressure[7]. The ZnO:Al was found to have a density of 5g/cm^3, a reduction compared to commonly reported values of 5.45g/cm^3. The density of the deposited SiO_x was found to be 2.15g/cm^3, lower than values expected for crystalline SiO_x confirming the amorphous nature of the films. The a-IGZO/SiO_x superlattices were found to have a low roughness of 0.5 nm at the a-IGZO and SiO_x interfaces. ZnO:Al/SiO_x superlattices were found to have a higher interface roughness of 1 nm. No change in density or surface roughness was observed between reference films and the superlattices. The oscillations arising from the total >150 nm thickness of the deposited superlattice are beyond the threshold resolvable by our system. As a result, the measured pattern consists of only signal from the individual layers allowing for significant reduction in the complexity of the fits. Illustrative examples of the fits obtained are given in Figure S1. The parameters extracted from the fits are given in Supplement S7.

S2. X-Ray Diffraction measurements of the superlattices

Representative X-Ray Diffraction (XRD) patterns of the superlattices are plotted in Figure S2. The reference a-IGZO film and superlattices are found to be fully amorphous regardless of SiO_x thickness. The ZnO:Al reference film and superlattices were all found to be highly textured along the [002] direction. This is consistent with previous results that demonstrated that the inclusion

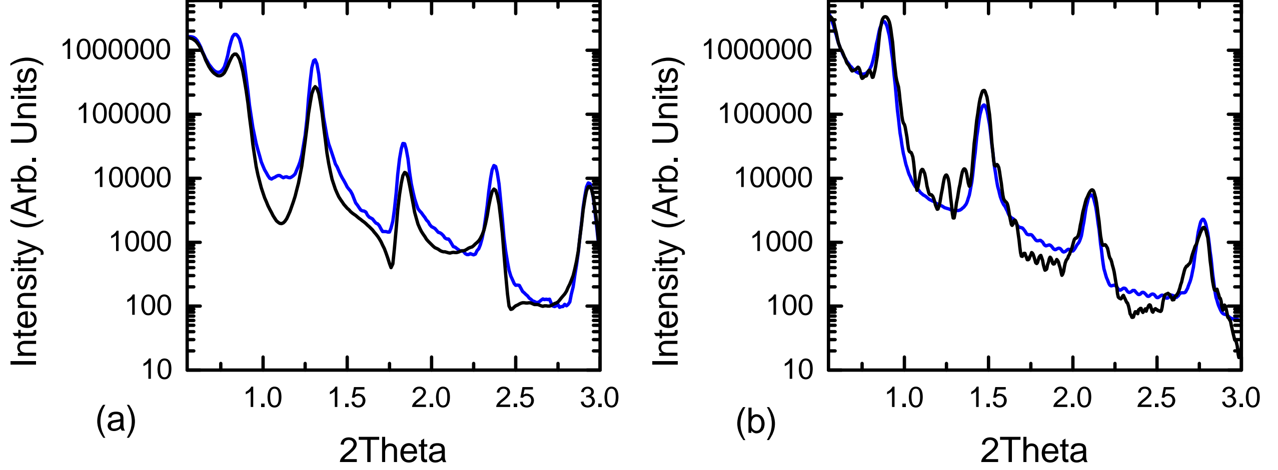

FIG. S1. | XRR fits of the deposited superlattices. XRR fits of the superlattices. **(a)** 10/**5 nm** a-IGZO/SiO_x **(b)** 10/**5 nm** ZnO:Al/SiO_x. (−) Gives the measured data. (−) Gives simulated data.

of a SiO_x buffer layer can serve to reset the crystallographic texture of the growing ZnO:Al film[8]. The dependence of the coherent domain size, as calculated by the Scherrer equation, on ZnO:Al thickness is plotted in the inset of Figure S2. The crystallite size in the 80 nm ZnO:Al film was on the order of 23 nm, while in the superlattices it was found to be on the order of the thickness of the ZnO:Al layer. This reduced crystallite size results from the vertical spacial confinement of the layers in the superlattices. No crystalline peaks from the SiO_x was observed in any superlattice.

S3. a-IGZO Composition

The composition of the a-IGZO target was measured via Energy Dispersive X-ray spectroscopy (EDX) and was found to have a In:Ga:Zn ratio of $1 : 1 : 1$. For the thin films, measurements (not shown here) of the In3d, Ga2p and Zn2p peaks were performed in order to obtain the composition of the a-IGZO. Films were found to be highly indium enriched, with the top contact of the deposited superlattices possessing a In:Ga:Zn ratio of $1 : 0.06 : 0.06$. The limited penetration depth of XPS measurements (≈ 5 nm) precluded the direct measurement of the In:Ga:Zn ratios of the sub-surface layers. Thus, in order to verify that no change in composition was occurring within the superlattice, the composition of a 10 nm a-IGZO film was compared to the final deposited layer of the superlattices. The variation was found to be negligible, indicating that composition remains consistent throughout the superstructure. This consistency is likely a result of our deposition methodology in which the power applied to the a-IGZO target was ramped down prior to the

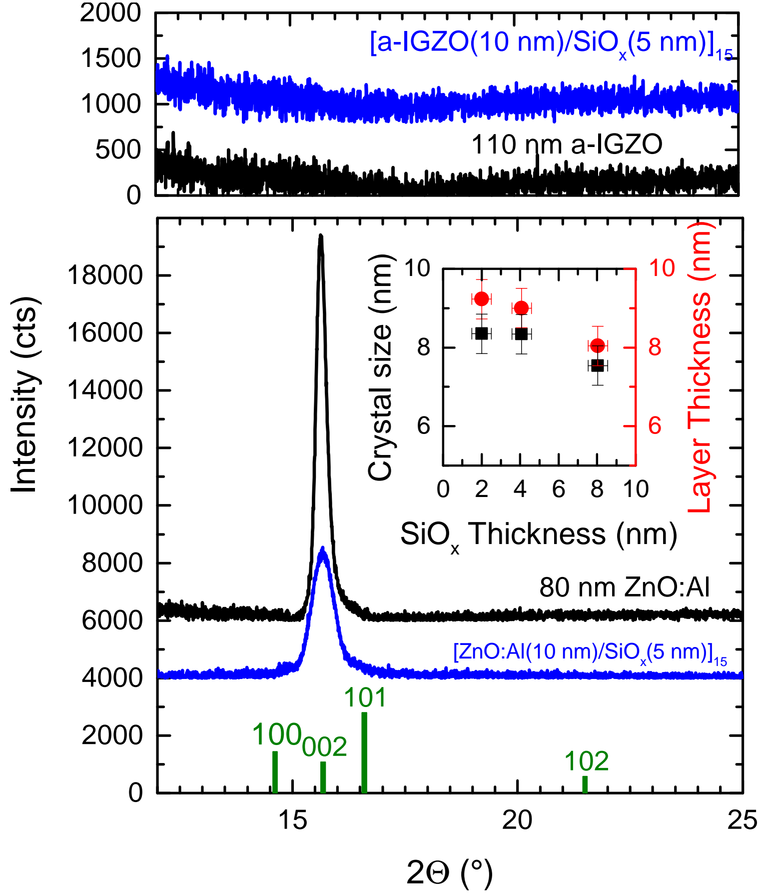

FIG. S2. | XRD of the deposited ZnO:Al and a-IGZO superlattices. XRD patterns of the deposited reference films and superlattices. The upper graph gives the XRD pattern of a (–) 110 nm a-IGZO film and (–) 10/**5 nm** a-IGZO/SiO$_x$ superlattice. The lower graph gives the XRD pattern of the ZnO:Al film and a representative ZnO:Al superlattice. The ZnO:Al is found to be highly textured along the [002] reflex while the a-IGZO is amorphous. (–) 80 nm ZnO:Al(–) 10/**5 nm** ZnO:Al/SiO$_x$ superlattice. Inset gives the ZnO:Al crystallite size as a function of the SiO$_x$ layer thickness (■). Both films possess an amorphous character. The individual ZnO:Al layer thickness obtained from XRR is plotted for comparison (●).

deposition of each layer, reseting the deposition conditions. A reduction in the indium enrichment and increase in the Ga content was detected in the 50 nm a-IGZO film, which possesses a In:Ga:Zn ratio of 1 : 0.18 : 0.06. While the mobility of a-IGZO is known to depend on the composition of the samples[9,10], little variation is observed as a result of this change.

S4. Experimental verification of homogeneous current distribution throughout the superstructure

In order to experimentally confirm that the SiO_x layers were not inhibiting the flow of current to the lower layers of the superlattices, two samples of identical SiO_x layer thicknesses but of different overall thicknesses were deposited for comparison. Two 10/10nm a-IGZO/SiO_xsuperlattices were grown and compared to a 10nm a-IGZO film. The first was 90nm thick overall while the second was 190nm thick. 10nm SiO_x layers were employed as that is the maximum thickness used in this work. Should the current be injected into the full superstructure, it would be expected that the resistivities of the two structures should be the same. Similarly, it would be expected that the sheet resistance of the superlattices would be inversely proportional to film thickness. Results differing from this would indicate that not all of the a-IGZO layers contribute equally to the electron transport and thus that current is not flowing through the full structure. The samples were deposited and annealed in the same manner as the other superlattices. The sheet resistance and resistivity of the deposited superlattices and reference 10nm film are given in Figure S3. It can be observed that the sheet resistance of the 90nm superlattice is half that of the 190nm superlattice leading to similar resistivity. In addition both superlattices display a sheet resistance different than that of a single 10nm a-IGZO film. This verifies that the SiO_x layers are do not appreciably inhibit current flow into the lower layers.

S5. Finite Element Method Simulations

Finite Element Method (FEM) simulations were performed in order to assess the conditions under which the low refractive index layer might inhibit the current distribution throughout the superstructure. The system can be modeled simply in two dimensions, treating the direction along the gold contacts as infinite. A 1 mm wide probe distance was simulated for a 10/10 nm periodicity superlattice film. The resistivity of the a-IGZO layers was selected as $6\times10^{-3}\,\Omega$cm and the SiO_x layers were varied in resistivity. An input boundary current was injected at the top surface on one end of the sample and allowed to leave through the top surface at the other end. Figure S4 gives the simulated current density distribution for a 10/10 a-IGZO/SiO_x superlattice for a variety of SiO_x resistivities. Little variation in the current density of the lower layers is observed below $10^7\,\Omega cm$. At SiO_x resistivities above $10^7\,\Omega cm$ the current is preferentially driven through the surface layer with smaller portions traveling through the subsequent a-IGZO layers. Current density is reduced

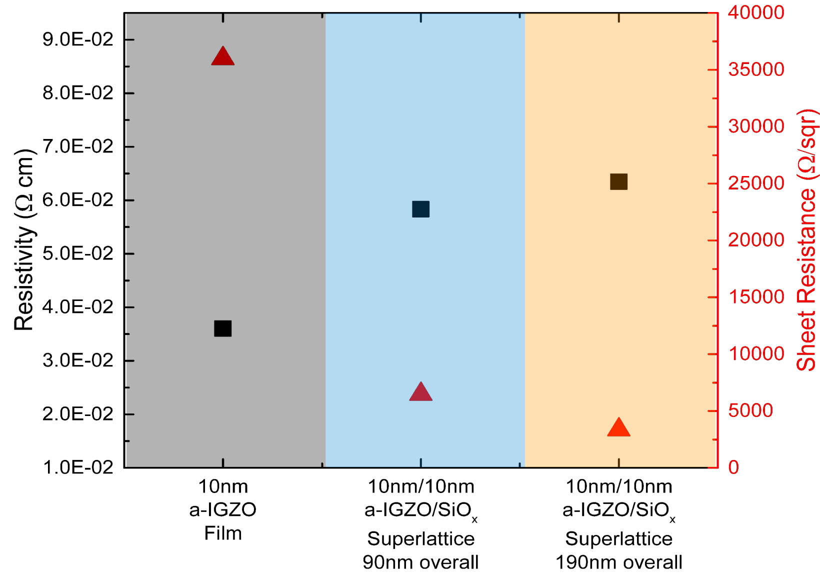

FIG. S3. | Comparison of 10/10 a-IGZO/SiO$_x$ superlattices grown to different overall thicknesses Sheet resistance and resistivity of a 10nm a-IGZO film and two superlattices of identical SiO$_x$ layer thickness grown to different total thicknesses. Shaded Grey area gives the 10nm a-IGZO film. Shaded blue area gives the 90nm total thickness superlattice. Shaded orange gives the 190nm superlattice. (■) Resistivity. (▲) Sheet resistance.

to close to zero within the SiO$_x$ layers. Thus the simulation indicates that provided the SiO$_x$ layer exhibits a resistivity below $10^7 \Omega cm$ the current density will be homogeneously distributed. This simulation gives the upper limits for the conductivities of the refractive index layer required to maintain homogeneous current distribution throughout the superstructure.

S6. Discussion of optical bandgap and the possibility of confinement effects

A blueshift in the bulk critical point energy of both superlattices can be observed in Figure 4 (Main article). Unfortunately, analysis of the higher energy range of the refractive index is complicated by the limited dynamic range of our ellipsometer. While a shift can also be observed in Tauc plots of the a-IGZO/SiO$_x$ superlattices grown on sapphire, the analysis is complicated by a shift in the structure of the onset of absorption due to the SiO$_x$ inclusion. Furthermore, as discussed in the main body of this work some of the films experience carrier concentration variation with SiO$_x$ layer thickness resulting in the superposition of the Burnstein-moss induced changes with any confinement resultant expansion. It has been shown that the a-IGZO/SiO$_x$ barrier should lead to

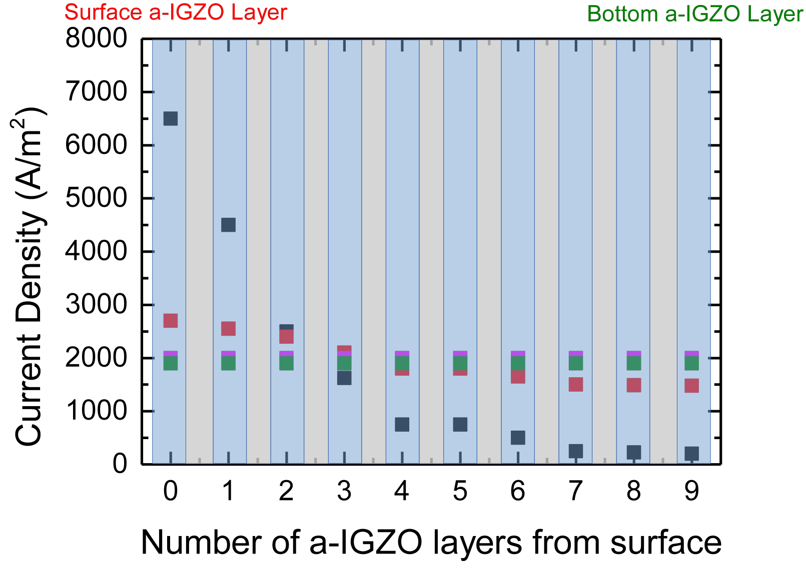

FIG. S4. | Simulation of the current density distribution within a 10/10 a-IGZO/SiO_x superlattice. Plot of the simulated current density in the a-IGZO layers from surface (left) to bottom (right).Graph is shaded blue for the a-IGZO layers and grey for the SiO_x. Current density drops to ≈ 0 for the SiO_x layers. Various resistivities of the SiO_x layers are simulated (■) 10^7 Ωcm, (■) 10^6 Ωcm, (■) 10^5 Ωcm , (■) 10^4 Ωcm

strong confinement[11]. However, experiments performed by Abe et al.[12] indicate that quantisation is unlikely to occur in a-IGZO layers of 10 nm thickness as used in this work. These complications prevent us from drawing a definitive conclusion regarding any possible optical bandgap shifts in the superlattices based on ellipsometry alone.

S7. Structure of the Deposited Superlattices

Tables SI, SII and SIII give the layer thickness, periodicity and electrical properties of the a-IGZO superlattices on glass, a-IGZO superlattices on sapphire and ZnO:Al superlattices on glass respectively. Quoted thicknesses are calculated from the fits of the XRR data.

a-IGZO/SiO_x layer thickness (nm) (nominal)	Number of layers (not including cap)	Total a-IGZO thickness overall (nm)	Total SiO_x thickness overall (nm)	Sheet Resistance ($\Omega\square$)	Mobility (cm^2/Vs)
110/0	1	100	0	597	16.5
11/2	15	176	30	9980	10.62
11/3	14	165	42	32000	7.34
11/3.8	13	154	49	25000	6.04
11/4.2	12	143	50	688	14
11/6.8	10	121	68	489	8.57
11/8.3	9	110	74	895	7.877

Table SI. | Composition and electrical properties of the a-IGZO/SiO_x superlattices deposited on glass

a-IGZO/SiO_x layer thickness (nm) (nominal)	Number of layers (not including cap)	Total a-IGZO thickness overall (nm)	Total SiO_xthickness overall (nm)	Sheet Resistance ($\Omega\square$)	Mobility (cm^2/Vs)
55/0	1	55	0	1100	16.08
9.8/2.4	15	156	30	4210	10.08
11/4.1	12	143	54	600	9.79
11/8.3	9	110	74	1254	5.96

Table SII. | Composition and electrical properties of the a-IGZO/SiO_x superlattices deposited on Sapphire

$ZnO:Al/SiO_x$ layer thickness (nm) (nominal)	Number of layers (not including cap)	Total ZnO:Al thickness overall (nm)	Total SiO_x thickness overall (nm)	Sheet Resistance (Ω□)	Mobility (cm^2/Vs)
81/0	1	81	0	428	7.31
9.2/2	15	148	30	652	5.05
8.9/4	12	116	48	594	4.14
8.2/8	9	82	72	2610	1.01

Table SIII. | Composition and electrical properties of the $ZnO:Al/SiO_x$ superlattices deposited on glass

References

[1]Fullerton, E. E., Schuller, I. K., Vanderstraeten, H. & Bruynseraede, Y. Structural refinement of superlattices from x-ray diffraction. *Phys. Rev. B* **45**, 9292 (1992).

[2]Payne, A. & Clemens, B. Influence of roughness distributions and correlations on x-ray diffraction from superlattices. *Phys. Rev. B* **47**, 2289 (1993).

[3]Barshilia, H. C., Selvakumar, N., Rajam, K., Gopinadhan, K. & Chaudhary, S. Investigation of interface properties of sputter deposited tin/crn superlattices by low angle x-ray reflectivity. *J. Phys. D: Appl. Phys.* **41**, 205409 (2008).

[4]Lamelas, F., He, H. D. & Clarke, R. Numerical modeling of superlattice x-ray-scattering intensities. *Phys. Rev. B* **43**, 12296 (1991).

[5]Huai, Y., Cochrane, R. & Sutton, M. X-ray-diffraction studies of co/re superlattices. *Phys. Rev. B* **48**, 2568–2576 (1993).

[6]Chowdhury, M. D. H., Um, J. G. & Jang, J. Remarkable changes in interface o vacancy and metal-oxide bonds in amorphous indium-gallium-zinc-oxide thin-film transistors by long time annealing at 250 c. *Appl. Phys. Lett.* **105**, 233504 (2014).

[7]Grochowski, J. *et al.* Origin of lower film density and larger defect density in amorphous in–ga–zn–o deposited at high total pressure. *Display Technology, Journal of* **11**, 523–527 (2014).

[8]Owen, J. I., Zhang, W., Köhl, D. & Hüpkes, J. Study on the in-line sputtering growth and structural properties of polycrystalline zno: Al on zno and glass. *J. Cryst. Growth* **344**, 12–18 (2012).

[9]Jeong, J. K. *et al.* High performance thin film transistors with cosputtered amorphous indium gallium zinc oxide channel. *Appl. Phys. Lett.* **91**, 3505 (2007).

[10]Hosono, H. Ionic amorphous oxide semiconductors: Material design, carrier transport, and device application. *J. Non-Cryst. Solids* **352**, 851–858 (2006).

[11]Douglas, E. *et al.* Measurement of sio_2/$inzngao_4$ heterojunction band offsets by x-ray photoelectron spectroscopy. *Appl. Phys. Lett.* **98**, 2110 (2011).

[12]Abe, K., Nomura, K., Kamiya, T. & Hosono, H. Optical evidence for quantization in transparent amorphous oxide semiconductor superlattice. *Phys. Rev. B* **86**, 081202 (2012).